
Multibody System Dynamics **7:** 285–305, 2002.

Optimal Design of Cams

A. CARDONA, E. LENS and N. NIGRO
Facultad Regional Santa Fe, Universidad Tecnológica Nacional, Lavaise 610, (3000) Santa Fe, Argentina; and Centro Internacional de Métodos Computacionales en Ingeniería (CIMEC-INTEC), Universidad Nacional del Litoral – CONICET, Güemes 3450, (3000) Santa Fe, Argentina

(Received: 3 January 2000; accepted in revised form: 28 February 2001)

Abstract. We present a methodology to design cams for motor engine valve trains using a constrained optimization algorithm. The imposed constraints are the maximum valve lift and timings while the objective function is to maximize the time integral of the valve area opened to gas flow. A piecewise analytically defined acceleration is imposed, so that the time instants controlling the profile of accelerations are used as variables for optimization. The strategy takes into account some geometrical constraints, e.g. to avoid interference between intake and exhaust valves, and between valves and piston. Also, minimum and maximum levels of acceleration are limited to avoid excessive forces in the mechanisms chain, and to prevent the possibility of separation between cam and follower. Once an optimal lift profile is determined, the cam shape is computed using an inverse kinematics analysis that takes into account all the geometric nonlinearities introduced by the kinematical chain. Finally, the whole mechanism is verified in a dynamics analysis to check satisfaction of the criteria for design. Comparisons with standard profiles of motion were made. Also, the profile was evaluated in an experimental device, where the actual valve displacement was measured.

Key words: cams, nonlinear dynamics, synthesis of mechanisms.

1. Introduction

Several factors should be considered in the design of motor engine valve trains and cams, which may be briefly classified into fluid dynamics and mechanical ones. The maximum valve lift and the valve timings are determined based on fluid dynamics considerations. Structural considerations are taken into account to satisfy these two factors, and at the same to time keep the structural integrity of the mechanism and optimize its performance. To this aim, efforts should be minimized to work within the allowable stress levels, and jumping between cam and follower should be avoided. At the same time, the gas flow through each valve should be maximized. Further complexity appears because of nonlinearities introduced by the kinematical chain usually interposed between cam and valve. Last but not least, the feasible solution space is restricted to avoid mechanical interferences.

The aim of this paper is to develop a systematic procedure for optimal cam design. After properly defining an optimization problem and solving it, we get a valve lift profile that is the input data to a mechanical synthesis phase of analysis, where we compute the cam profile required to reach the desired valve motion.

Finally the whole mechanical system is dynamically analyzed in order to validate the operation conditions.

Methods for cam motion synthesis have become increasingly sophisticated and many alternatives are continuously proposed [1, 4, 12, 13, 17, 19, 22, 23]. In a previous work, we presented a method to analyze the kinematics and dynamics of mechanisms with cams [2], using splines for describing cams geometry. In this work, an original software to obtain an optimal valves motion is combined with the program for mechanisms analysis. In this way, the analyst is allowed to synthesize a cam profile that takes into account the geometrical nonlinearities introduced by the kinematical chain.

2. Fluid Dynamics Design Factors

The flow field within the cylinder of internal combustion engines is the most important factor controlling the combustion and engine breathing processes. Both phenomena are central keys in the determination of the engine efficiency.

One of the main unknowns in valves train design is the maximum valve lift (L). Other important design factors are the valve timings: the valve opening and closing angles θ_{VO} and θ_{VC}.

Predicting the influence of the maximum valve lift and valve timings over flow motion is a difficult task, not only from the theoretical but also from the experimental point of view. Increasing the maximum valve lift and the time interval in which the valve remains open does not guarantee better operation conditions at all. Even though the valve geometric area A is increased when the two above mentioned parameters are increased, there are some other phenomena to be taken into account, the most important of which being the discharge coefficient C_D which defines an effective flow area ($A_e = C_D A$) including how the fluid dynamic patterns alter the cross section through which the flow motion is established [8].

The roles of valve lift and timings are very important for the turbulence level inside the combustion chamber. These factors control both the burning rate through the flame front speed and the heat losses affecting mainly the thermal efficiency. Also, the valve overlap defined by valve timings is a very important parameter because of its influence over the tuning of the intake and exhaust systems.

Because of the lack of accurate information about the fluid dynamics pattern through the intake, combustion chamber and exhaust, designers make use of the flowmeter very often. This is a static experimental device to measure flow and set up roughly the maximum valve lift, together with some other geometrical factors such as valve body dimensions, seats configuration and port details. Practical experiences recommend the maximum value of valve lift to be bounded at a 40% of the valve diameter at most.

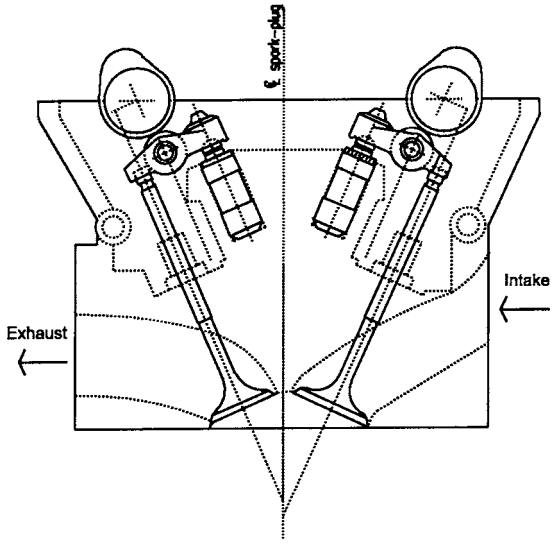

Figure 1. Schematic view of intake and exhaust valves and piston.

3. Mechanical Design Factors

Among the various mechanical design factors that influence the design of cams for motor engine valve trains, we take into consideration geometrical interferences and dynamic forces.

3.1. INTERFERENCES

The intake valve opening and exhaust valve closing are carried out in the neighbourhood of the piston top dead centre (TDC). Since the distances between valves-piston and also valves themselves are very small, it is necessary during the design of valve motion to detect and avoid any possible geometrical interference. This factor is very critical especially in engines with large valves overlapping. Figure 1 shows a detail of the intake and exhaust valves and camshafts for the particular motor engine that we analyze as an example of application in this paper.

3.2. DYNAMICAL FORCES

In order to reach the maximum valve lift L in the time interval where the valve remains open, we need to specify a motion profile that satisfies not only the above mentioned interference constraints but also the following dynamics restrictions [18]:

1. no jumping between cam and follower,
2. no impact in the valve seating,

3. maximum stresses bounded for reliability and minimal wear.

The spring dynamics also plays a fundamental role in high speed cam follower systems. At high-speeds, springs may lose force due to an internal resonance. This resonance may be excited by high-order harmonics of the cam lift at any speed.

Distributed-parameter models of the spring have been proposed to simulate the spring dynamics [6, 10, 14, 16, 20]. Modelling of coil clash phenomena has been taken into account using a moving boundary technique [11]. Furthermore, spring designs with variable cross section have also been proposed to minimize amplitude of spring resonance [9]. Nested springs are used to introduce dissipation by Coulomb friction between inner and outer spring coils, and damp internal resonance. The estimation of friction values is a difficult task, so various forms of predicting them have been proposed [6, 21].

4. Constrained Optimization Strategy

4.1. PARAMETERIZATION OF VALVES MOTION

Motion in time of motor valves follows the general description of figure 2. We may distinguish five zones: initial ramp, acceleration, spring-control, deceleration, and final ramp. Ramps are designed to strike the cam-follower at a given velocity and to allow some amount of clearance between cam and follower at the closed position. At the end of the ramp, the valve is accelerated by a curve of increasing slope. The curve should be such that transmitted load does not suffer sudden changes and the valve effectively follows the cam. While moving under spring control, the valve decelerates up to reaching zero velocity and then accelerates downward until closing, passing through a deceleration zone and final ramp [18].

The maximum values of positive acceleration are limited by the maximum efforts the system can sustain. On the other hand, during the spring-controlled zone, the negative acceleration imposed by the cam profile should be smaller than a given limit in order to make the inertia load a fraction of the available spring force and avoid jumping.

As we have mentioned before, fluid dynamics factors are out of the scope of the present paper, and both the maximum valve lift L and the valve timings θ_{VO} (valve opening angle) and θ_{VC} (valve closing angle) are assumed as input data, with θ being the crank angle.

We parameterize valve motion by imposing a smooth profile of acceleration as follows:

$$a(\theta) = \sum_{j=1}^{N} a_j(\theta), \tag{1}$$

where

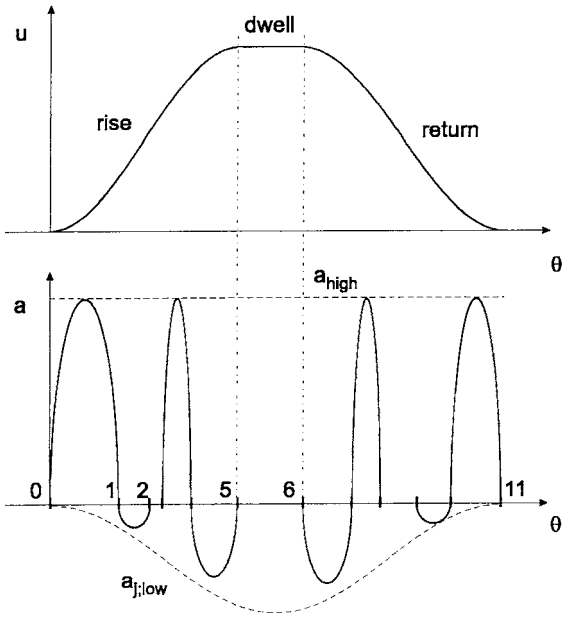

Figure 2. Valves motion diagram.

$$a_j(\theta) = \begin{cases} 0, & \theta < \theta_{j-1}, \\ \overline{a}_j[1 - \mathrm{e}^{-\overline{\lambda}(\theta-\theta_{j-1})}], & \theta_{j-1} \le \theta \le \theta_{0.5}, \\ \overline{a}_j[1 - \mathrm{e}^{-\overline{\lambda}(\theta_j-\theta)}], & \theta_{0.5} < \theta \le \theta_j, \\ 0, & \theta > \theta_j, \end{cases} \tag{2}$$

with

$$\overline{\lambda} = \frac{\lambda}{\alpha_j}, \quad \theta_{0.5} = \frac{\theta_{j-1} + \theta_j}{2}, \tag{3}$$

where α_j is the length of the interval $[\theta_{j-1}, \theta_j]$. Function $a_j(\theta)$ can be seen as a smoothed rectangular profile, with support $[\theta_{j-1}, \theta_j]$ and height $\overline{a}_j$. Parameter λ controls smoothness (and thus jerk): for large values of λ we get accelerations which are closer to a rectangular profile. In practice we use a value of $\lambda = 7$, which gives us a smooth enough accelerations profile.

Velocities and displacements can be obtained by time integration, giving:

$$v_j(\theta) = v_{j-1} + \begin{cases} \frac{\overline{a}_j}{\omega}\left[\theta - \theta_{j-1} - \frac{1-\mathrm{e}^{-\overline{\lambda}(\theta-\theta_{j-1})}}{\overline{\lambda}}\right], & \theta_{j-1} \le \theta \le \theta_{0.5}, \\ \frac{\overline{a}_j}{\omega}\left[\theta - \theta_{j-1} + \frac{1-\mathrm{e}^{-\overline{\lambda}(\theta_j-\theta)}}{\overline{\lambda}} - 2\frac{1-\mathrm{e}^{-\lambda/2}}{\overline{\lambda}}\right], & \theta_{0.5} < \theta \le \theta_j, \\ \frac{\overline{a}_j}{\omega}\chi\alpha_j, & \theta = \theta_j, \end{cases} \tag{4}$$

$$u_j(\theta) = u_{j-1} + v_{j-1}(\theta - \theta_{j-1}) + \begin{cases} \frac{\overline{a}_j}{\omega^2}\left[\frac{(\theta-\theta_{j-1})^2}{2} - \frac{\theta-\theta_{j-1}}{\overline{\lambda}} + \frac{1-e^{-\overline{\lambda}(\theta-\theta_{j-1})}}{\overline{\lambda}^2}\right], & \theta_{j-1} \le \theta \le \theta_{0.5}, \\ \frac{\overline{a}_j}{\omega^2}\left[\frac{(\theta-\theta_{j-1})^2}{2} - \frac{\theta-\theta_{j-1}}{\overline{\lambda}} + \frac{2e^{-\lambda/2}(\theta-\theta_{0.5})}{\overline{\lambda}}\right. & \\ \qquad \left. + \frac{1-e^{-\overline{\lambda}(\theta_j-\theta)}}{\overline{\lambda}^2}\right], & \theta_{0.5} < \theta \le \theta_j, \\ \frac{\overline{a}_j}{\omega^2}\chi\alpha_j^2/2, & \theta = \theta_j, \end{cases} \tag{5}$$

with

$$\chi = 1 - \frac{2}{\lambda}(1 - e^{-\lambda/2}). \tag{6}$$

We may distinguish three zones in valve motion: rise, upper dwell and return. We use five segments to parameterize the rise and return, and one additional segment to parameterize the flat zone, as it can be seen in Figure 2. Acceleration amplitudes $\overline{a}_j$, $j = 1, 11$ are fixed *a priori*, in the form

$$\overline{a}_j = \begin{cases} a_{\text{high}}, & j = 1, 4, 8, 11, \\ a_{j;\,\text{low}}, & j = 2, 5, 7, 10, \\ 0, & j = 3, 6, 9, \end{cases} \tag{7}$$

where a_{high} is determined so that the maximum contact force does not exceed an admissible value, and $a_{j;\,\text{low}}$ is fixed in terms of the valve system mass and the spring constant, to avoid separation between cam and follower:

$$a_{j;\,\text{low}} = -\frac{k_{\text{spr}}}{\overline{m}} \min_{\theta\in[\theta_{j-1},\theta_j]} L_v^*(\theta), \quad j = 2, 5, 7, 10, \tag{8}$$

with k_{spr} being the spring stiffness and $\overline{m}$ an equivalent mass which takes into account masses of the valve, spring and rocker arm; $L_v^*(\theta)$ is a target valve lift profile defined as:

$$L_v^*(\theta) = L \sin^2\left(\pi \frac{\theta - \theta_{\text{VO}}}{\theta_{\text{VC}} - \theta_{\text{VO}}}\right). \tag{9}$$

In practice, values for $a_{j;\,\text{low}}$ are iterated in order to get reasonable minimal accelerations that avoid false valve motion due to jumping.

Valve motion is therefore parameterized in terms of the set of angles θ_j, $j = 0, \ldots, 11$. These parameters are not independent, and we may extract a subset of only six free parameters using the following considerations:

1. The initial and final angular displacements θ_0 and θ_{11} are equal to the valve opening and closing angles θ_{VO} and θ_{VC}.

2. During the rise phase, the motion profile should verify the conditions:

$$u(\theta_0) = h_{\text{ramp}}, \quad v(\theta_0) = v_{\text{ramp}}, \quad u(\theta_5) = L, \quad v(\theta_5) = 0. \tag{10}$$

3. During the return phase, the motion profile should verify the conditions:

$$u(\theta_6) = L, \quad v(\theta_6) = 0, \quad u(\theta_{11}) = h_{\text{ramp}}, \quad v(\theta_{11}) = -v_{\text{ramp}}. \tag{11}$$

Here, h_{ramp} and v_{ramp} are the height and velocity of the quietening ramps (at the design speed). Ramps are added to ensure that the valve contacts the valve seat at a maximum speed equal to v_{ramp}, low enough to minimize impact forces and avoid jumps, regardless of the actual value of clearance [7]. Typical values of valve velocity are approximately 0.4/0.6 m/sec, and clearance of about 0.1/0.2 mm is used between cam and follower.

From the conditions mentioned for the rise phase, angles θ_4 and θ_5 can be eliminated from the set of independent parameters. After some algebra, we get the relationships:

$$\theta_4 = \theta_3 + \left(\frac{\Delta_{45} - v_3}{|\overline{a}_4|\chi}\right)\omega, \tag{12}$$

$$\theta_5 = \theta_4 + \left(\frac{\Delta_{45}}{|\overline{a}_5|\chi}\right)\omega, \tag{13}$$

where

$$\Delta_{45} = \sqrt{\frac{v_3^2 + 2(L - u_3)\overline{a}_4\chi}{1 - \overline{a}_4/\overline{a}_5}} \tag{14}$$

and $v_3 = v(\theta_3)$, $u_3 = u(\theta_3)$. Similar relations are derived for the return zone:

$$\theta_7 = \theta_8 - \left(\frac{\Delta_{78} + v_8}{|\overline{a}_8|\chi}\right)\omega, \tag{15}$$

$$\theta_6 = \theta_7 - \left(\frac{\Delta_{78}}{|\overline{a}_7|\chi}\right)\omega, \tag{16}$$

where

$$\Delta_{78} = \sqrt{\frac{v_8^2 + 2(L - u_8)\overline{a}_8\chi}{1 - \overline{a}_8/\overline{a}_7}} \tag{17}$$

and $v_8 = v(t_8)$, $u_8 = u(\theta_8)$.

Finally, the selected values for parameterization of motion are the three first intervals lengths plus the last three intervals lengths, i.e.:

$$\boldsymbol{\alpha}^\star = \left\{ \begin{array}{c} \alpha_1 \\ \alpha_2 \\ \alpha_3 \\ \alpha_9 \\ \alpha_{10} \\ \alpha_{11} \end{array} \right\}. \tag{18}$$

The interval lengths are chosen as independent variables for the optimization problem for many practical reasons, e.g. to easily assign initial values (usually, $\boldsymbol{\alpha}^\star = \mathbf{0}$ provides a good starting point).

4.2. OPTIMIZATION

The objective of the design is to maximize the area below the lift curve, in order to maximize the net flow income. Let us define :

$$A = \int_{\theta_{\mathrm{VO}}}^{\theta_{\mathrm{VC}}} u(\theta)\, \mathrm{d}\theta. \tag{19}$$

The integral in (19) can be evaluated as $A = \sum_{j=1,11} A_j$, with:

$$A_j = \int_{\theta_{j-1}}^{\theta_j} u_j(\theta)\, \mathrm{d}\theta = A_{j-1} + u_{j-1}\alpha_j + v_{j-1}\frac{\alpha_j^2}{2} + \frac{\overline{a}_j}{\omega^2}\chi_1\frac{\alpha_j^3}{6} \tag{20}$$

and

$$\chi_1 = 1 - \frac{12 - 6\,\mathrm{e}^{-\lambda/2}}{4\lambda} + \frac{6\chi}{\lambda^2}. \tag{21}$$

The definition of the optimization problem is completed with the set of constraints:

1. *No interference between valve and piston*: the piston displacement with respect to the closed position of the valve, projected along the valve axis, may be written as:

$$x(\theta) = \Delta + \left(a_c(1 - \cos\theta) + l_b - \sqrt{l_b^2 - a_c^2 \sin^2\theta} \right) \cos\beta, \tag{22}$$

where a_c is the crank radius, l_b is the connecting-rod length, Δ is the free displacement of the valve when the piston is at the TDC ($\theta = 0$), and β is the angle between the valve axis and the piston axis. Then, the condition of non-interference may be expressed in the form:

$$u(\theta) - x(\theta) \leq 0. \tag{23}$$

2. *No interference between the valves themselves*: in order to avoid interference between one valve with the other, we first determine the valves displacements $\overline{u}_{\text{int}}, \overline{u}_{\text{exh}}$ for which each valve touches the other. Then we compute the intake valve displacement profile without any particular constraint. Afterwards, we calculate the exhaust valve displacement profile which verifies

$$u(\theta) < \overline{u}_{\text{exh}}, \quad \forall \theta > \overline{\theta}_{\text{int}}, \tag{24}$$

where $\overline{\theta}_{\text{int}}$ is the crank angular displacement from which $u(\theta) > \overline{u}_{\text{int}}$ at the intake valve.

3. *Positive interval lengths*: the interval lengths α_j, $j = 1, 11$ should be greater than or equal to zero, i.e.

$$\alpha_j \geq 0, \quad j = 1, \ldots, 11. \tag{25}$$

Note that this restriction applies to all interval lengths, and not only to those forming the set of unknowns $\boldsymbol{\alpha}^\star$.

4. *Positive valve displacement*: the computed valve displacement should be greater than zero, i.e.

$$u(\theta) \geq 0. \tag{26}$$

The objective function and restrictions are scaled so that the optimization problem is well defined. To this end, reference values of area, displacement and angular increments are defined as follows:

$$\begin{aligned} A_{\text{ref}} &= L\,(\theta_{\text{VC}} - \theta_{\text{VO}})\,/2, \\ u_{\text{ref}} &= L, \\ \alpha_{\text{ref}} &= (\theta_{\text{VC}} - \theta_{\text{VO}})\,/200. \end{aligned} \tag{27}$$

An optimization problem is therefore defined, whose solution

$$\boldsymbol{\alpha}^\star_{\text{opt}} = \arg\max A(\boldsymbol{\alpha}^\star) \tag{28}$$

is computed using standard routines for constrained optimization.

Note that the gradients of the objective function and of the constraints are not easy to compute analytically. Therefore, we use a constrained optimization strategy where these gradients are evaluated by finite differences. One important aspect is to appropriately program the analytical expressions above, so that the resulting objective function and constraints are differentiable. For instance, the routine should be able to give correct values even if the interval lengths are negative, a situation which may arise during computation of gradients (see the constraint equation (25)).

5. Cams and Valves Train Design and Analysis

The valves train of the motor engine shown in Figure 1 are taken as example. Figure 3 shows schematic drawings of the whole mechanical system and a detail

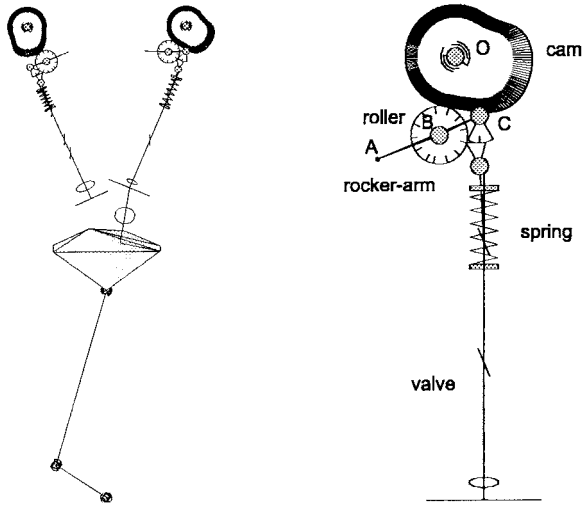

Figure 3. Overview of the mechanism model. Left: global view. Right: Detail of the intake subsystem.

of the intake subsystem. These plots correspond to the mechanism models made with the software *Mecano* [2, 3, 15] used for making the analysis. The cam, which axis is centered at point O, is in contact with the rocker-arm roller centered at B. The follower is fixed in the pivot rocker-arm A. Note that there is a small cam at the end of the rocker-arm which is in contact with a thrust piece at the top of the valve stem. Some important data are intake valve diameter 34.5 mm, exhaust valve diameter 29.0 mm, roller radius 8.5 mm, spring stiffness 31.4 N/mm, spring mass 48.5 g, spring preload 392 N, valve mass 58 g, rocker-arm mass 43 g.

5.1. VALVE LIFT OPTIMIZATION

First of all, the valve lift profile is computed following the optimization strategy described in Section 4.2. The valves timing imposed for the computation is: advance to the intake open angle 55°, delay to the intake close angle 72°, advance to the exhaust open angle 75°, and delay to the exhaust close angle 45°. The maximum lifts imposed are: intake 13.4 mm and exhaust 12.3 mm (these values correspond to the suggested lift-diameter valve ratio of 40%). The maximum positive acceleration used is 17000 m/sec^2 (intake) and 15000 m/sec^2 (exhaust).

Figure 4 plots the computed displacements for the intake and exhaust valves, where we can appreciate that lift design values of 13.4 and 12.3 mm are obtained. We also display the piston displacement, and we can see that there is no interference between piston and valves. Figures 5 and 6 present the velocity and acceleration profiles for both valves, at the maximum motor speed of 8500 rpm.

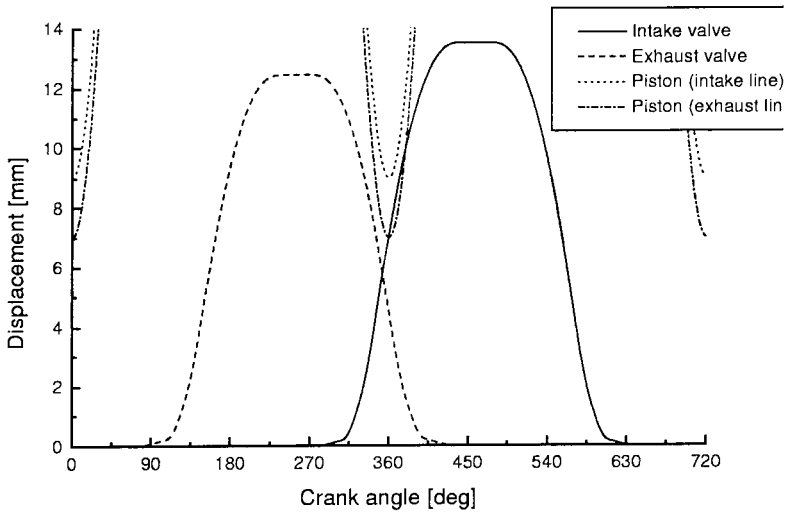

Figure 4. Intake valve displacement (solid line) and exhaust valve displacement (dashes). Dots show the piston displacement.

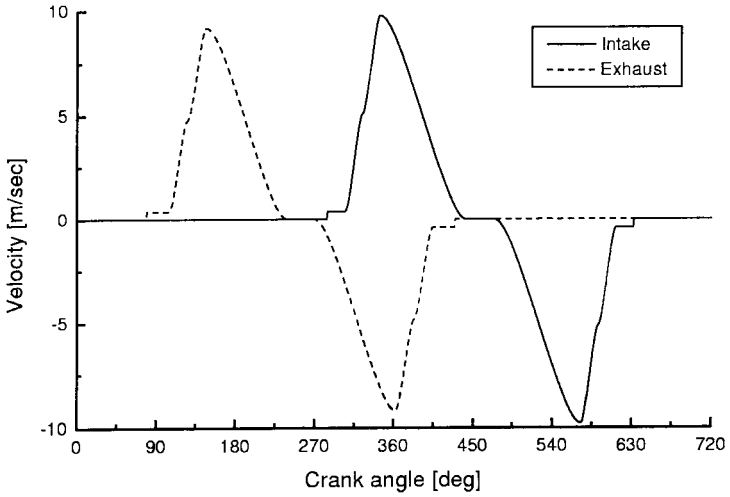

Figure 5. Velocity profile for the intake valve (solid line) and for the exhaust valve (dashes) at 8500 rpm.

5.2. CAM SYNTHESIS

Using the valve displacement profile relative to the crank angle (obtained from the optimization stage) as input data, we get the cams profile necessary to produce the desired valves motion.

This analysis is performed using the software *Mecano* [3, 15]: an inverse kinematical analysis is made imposing an adequately synchronized motion of valves and shafts, in a mechanism model without cams. As a result of the analysis, we

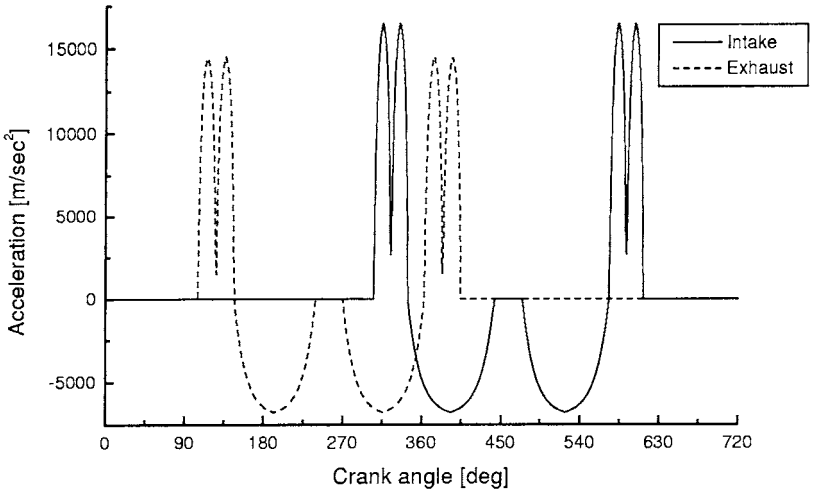

Figure 6. Acceleration profile for the intake valve (solid line) and for the exhaust valve (dashes) at 8500 rpm.

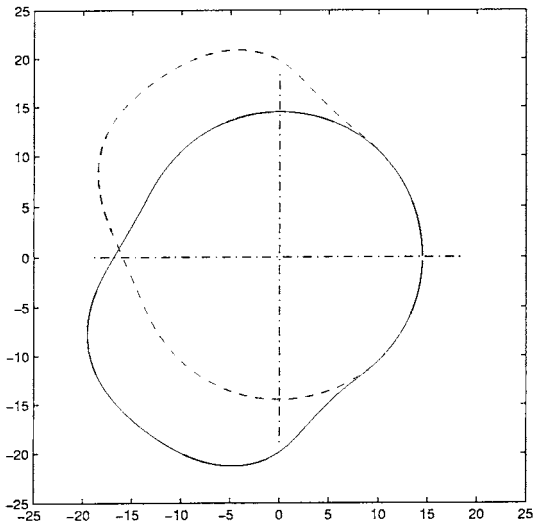

Figure 7. Cam profiles computed by synthesis, intake (solid line) and exhaust (dashes).

calculate the distance between cam and roller centers, as a function of the cams angular displacement. So as to consider the rocking motion of the rocker-arm, we compute also the relative angular position of the roller center with respect to the cam center, in terms of the cams angular displacement. From these two measures, a simple geometrical analysis gives us the cam profiles.

Figure 7 shows the obtained intake and exhaust cam profiles. It is interesting to note that, even though both motion profiles are symmetric, e.g. rise and re-

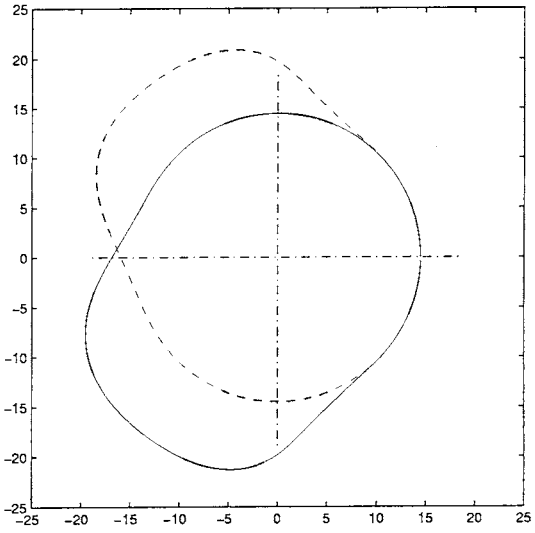

Figure 8. Cam profiles computed after correction of concavities, intake (solid line) and exhaust (dashes).

turn phases are almost mirrored, the resulting cams are not symmetric because of the geometric nonlinearities introduced by the rocking-arm and roller in the kinematical chain.

The cams profile is described in *Mecano* using a spline interpolation in polar coordinates [2]. To this end, the user enters a set of pairs $\{r_i, \theta_i\}$: using these points, a C_2 cubic spline interpolation is performed passing through this dataset (we note that the same description served to manufacture the cam master).

The above computed profiles are corrected to avoid negative curvature zones, so as to allow manufacturing for a given grinding wheel minimum radius. Since the computed profiles do not have large concavities, we use a fairly simple procedure of *straightening* the concave zones, followed by a spline smoothening in which radius r_i is corrected within a given tolerance in order to minimize the norm of the second derivative of the curve. Figure 8 shows the final intake and exhaust cams profiles.

5.3. DYNAMIC ANALYSIS

Finally a dynamic analysis is performed, assembling the two cams in the whole mechanism shown in Figure 3. The goal of this computation is to check the operation condition of the whole mechanical system, specially to verify that the modifications with respect to the nominal cam do not affect dynamic performance; there is no separation between cam and follower and efforts in each member remain within allowable values.

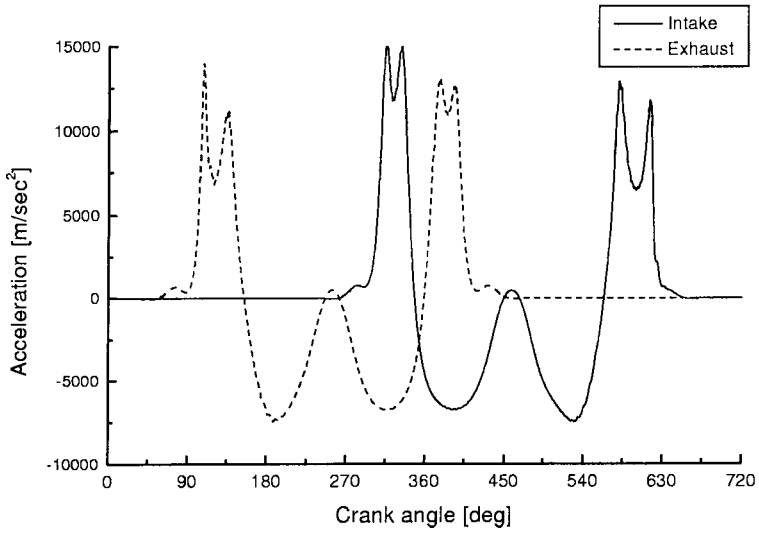

Figure 9. Valves accelerations, intake valve (solid line) and exhaust valve (dashes) at 8500 rpm.

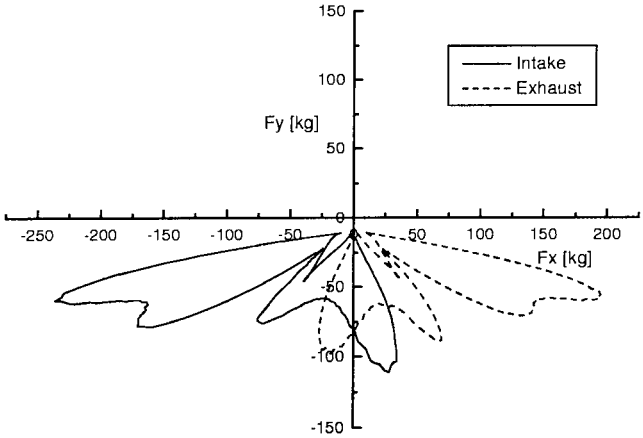

Figure 10. Time evolution of the horizontal and vertical components of reactions at the pivot rocker arm, intake valve (solid line) and exhaust valve (dashes), at 8500 rpm.

Cams are modelled following the approach presented in [2]. Contact between cam and follower is represented using a contact stiffness and damping, which can be assimilated to Hertz deformation. The rocker-arm elasticity was neglected in the analysis.

Figure 9 shows the acceleration profiles obtained by the dynamic analysis, which are in good agreement with those computed in the optimization stage (see Figure 6). The observed differences are mainly due to the cam smoothening process.

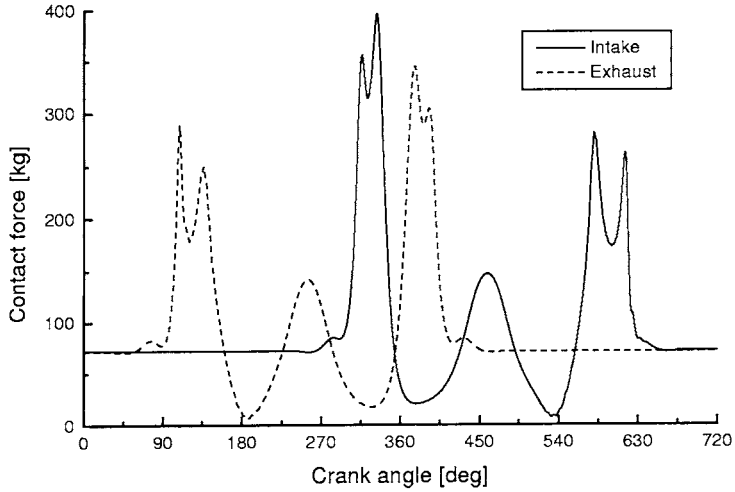

Figure 11. Contact force between roll follower and cam, intake valve (solid line) and exhaust valve (dashes) at 8500 rpm.

Figure 10 plots the reactions at the pivot rocker arm that arise from the dynamic response of the follower to the cam motion. These values of forces compared to those obtained from dynamic analysis with the present cam in use are found acceptable.

Figure 11 shows the time evolution of the contact forces at cam-follower. We clearly see that no jumping appears throughout the whole engine cycle, since the computed values are always positive.

6. Comparison of the Synthesized Profile with Other Profiles of Motion

There is a large variety of profiles proposed for cam motion in high-speed mechanisms: cycloidal, harmonic, polynomial [23], trigonometric series [22], rational B-splines [19], Bernstein–Bezier harmonics [17], trigonometric splines [13], etc. Several criteria may be used in order to establish a comparison, e.g.:

- maximum acceleration,
- harmonic content,
- residual vibration.

We compared our profile with the standard cycloidal and with the polynomial 2–3 proposed by Yu and Lee [23], by analyzing the downward phase from maximum to zero lift. Curves were normalized to unit lift and angle interval $0 \leq T \leq \pi$. Also, a little upper dwell zone was added to the cycloidal and Yu and Lee profiles to get the same value of area below the lift curve. We may appreciate that our profile and Yu and Lee's close faster than the cycloidal profile of motion (Figure 12).

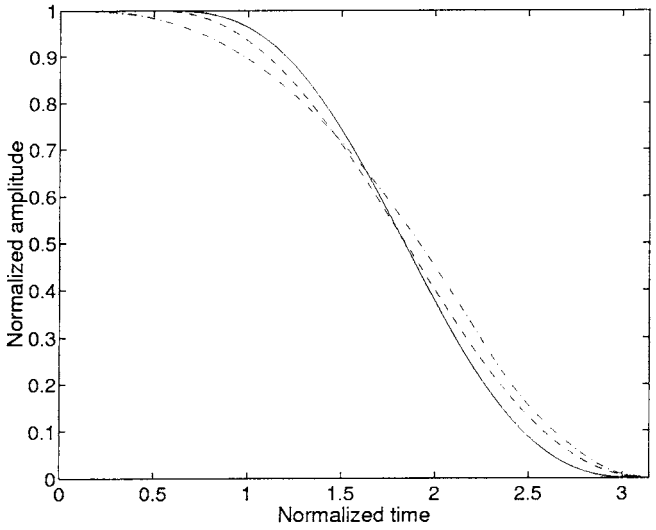

Figure 12. Valve motion normalized profile at downward zone. Comparison between cycloidal (solid line), Yu and Lee polynomial (dashes) and our profile (dashes and dots).

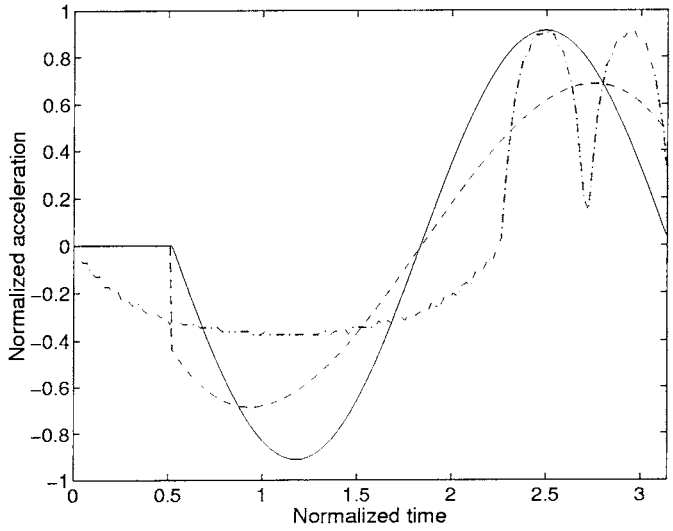

Figure 13. Normalized valve accelerations profile at downward zone. Comparison between cycloidal (solid line), Yu and Lee polynomial (dashes) and our profile (dashes and dots).

Figure 13 displays the accelerations for the same three profiles. We may appreciate that the acceleration level at the spring-controlled zone is much higher in the cycloidal and in the Yu and Lee profiles than in ours with the consequent larger tendency to produce jumping.

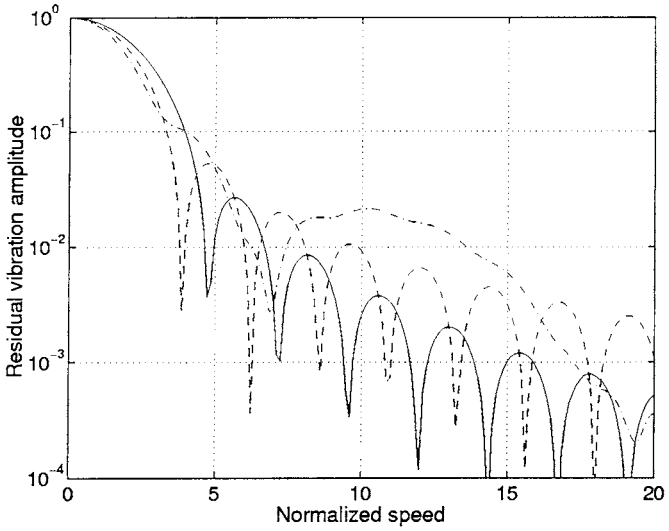

Figure 14. Residual vibration amplitudes. Comparison between cycloidal (solid line), Yu and Lee polynomial (dashes) and our profile (dashes and dots).

The tendency for a motion to excite vibration of the spring may be characterized through the response of a single degree of freedom cam follower system. The residual vibration spectrum is plotted as a function of the normalized operating speed $F = f\theta/\pi\omega$, where f is the oscillator frequency [rad/sec], θ is the down angle [rad] and ω is the camshaft speed [rad/sec].

Figure 14 plots the residual vibration spectra for the profiles of motion in study. We may see that if we increase the angular speed or the spring mass, F decreases and we get larger values of the residual vibration amplitude. The residual vibration is increased also when the spring is softened. Typical values of F for our configuration at maximum speed are in the order of $F = 2$. We may see that the residual vibration amplitude given by our profile is more or less the same as that given by the Yu and Lee profile, which they recommend for high speed applications. The cycloidal profile, though having a lower vibration level at low speeds, gives higher excitation levels at this regime.

7. Experimental Validation

A cam synthesized following the described methodology was built and experimented. For this purpose, a master cam was cut from a profile described by a spline curve, and a camshaft was built in a copying grinding machine. We remark that cam profile errors can have a large influence on the dynamic performance of high-speed follower cam systems [5].

We should mention that the cam used for the experiences does not correspond exactly to the one shown in previous sections. For instance, a maximum crankshaft

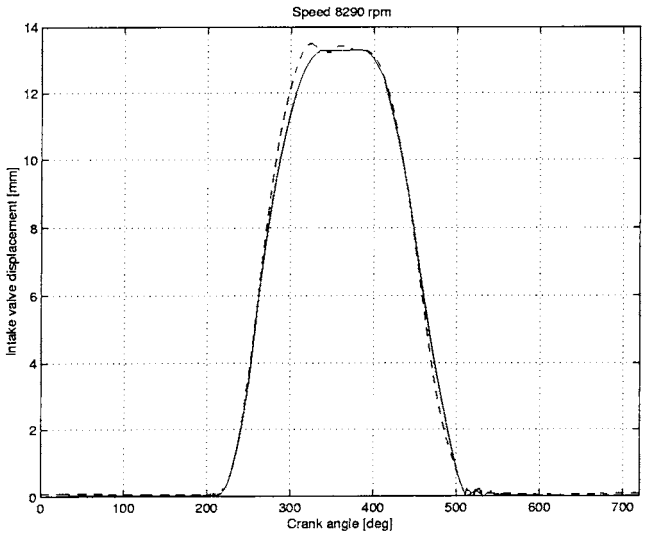

Figure 15. Intake valve displacement at 8290 rpm: nominal motion (continuous line), measured motion (dashed line).

speed of 8300 rpm was used in computations, which corresponds to the speed set at the electronic limit of the motor engine, and slightly different valve timings were used.

In order to analyze the dynamic behaviour of the cam-follower system, an experimental setup was used where the camshaft was electrically driven, and the valve displacements were measured using an optical position transducer. Pressurized motor oil from an external pump was fed into the experimental setup to lubricate the valve train in the usual manner. A shaft encoder recorded angular displacements.

The valve train was operated at speeds up to 8900 crankshaft rpm. Figure 15 displays the displacements time evolution of the intake valve measured at 8290 rpm. We may appreciate that there are small differences between the designed valve lift and the actual lift. The valve is beginning to *float* at the upper dwell and also, there is a small valve bounce when it returns to seat.

We should mention that these measurements may have been influenced by errors introduced during manufacturing of this camshaft specimen (i.e. the ramps were not copied correctly). Nevertheless, we think the displayed measures serve quite well as an overall indicator of dynamic performance.

The camshafts were installed into the engine. Experiences have shown some improvements in torque and power measurements over previously used cams designs (differences of nearly 4% were evidenced). Clearly, this fact is only an indication of feasibility of the proposed procedure.

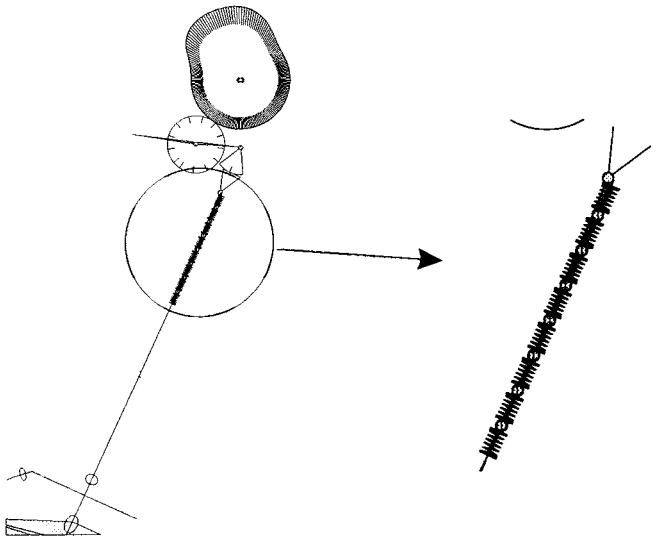

Figure 16. Detail of finite element model of spring at the intake valve.

8. Spring Dynamics

The effects introduced by the internal dynamics of the spring are analyzed using a discrete valve spring dynamics model, similar to the one used by Schamel et al. [16]. We take into account coil clash and Coulomb friction between inner and outer springs. To this end, each spring (inner and outer) is represented by eight springs in series. Coils clash is modeled as a varying stiffness, with a contact stiffness equal to 10000 times the stiffness of the spring. Coulomb friction is modeled by considering a friction damper lumped at each internal node (see Figure 16). The friction force was estimated from static measurements on the actual springs.

Figure 17 displays the evolution of the computed contact force between cam and follower, for two cycles. If we compare this figure with Figure 11, we can see the spring oscillations superposed to the contact force evolution computed using a linear spring model. These oscillations are damped, after valve closing, by internal friction forces.

We can also appreciate that at crank angular displacements equal to 400 deg and multiples, high frequency vibrations excited by coils clash develop. These vibrations are damped when coils come into contact at maximum lift. We think these vibrations can be at the origin of the separation observed during the experiences (see Figure 15), but further experiences are needed in order to get a definitive conclusion. In particular, it would be of interest to monitor the contact forces.

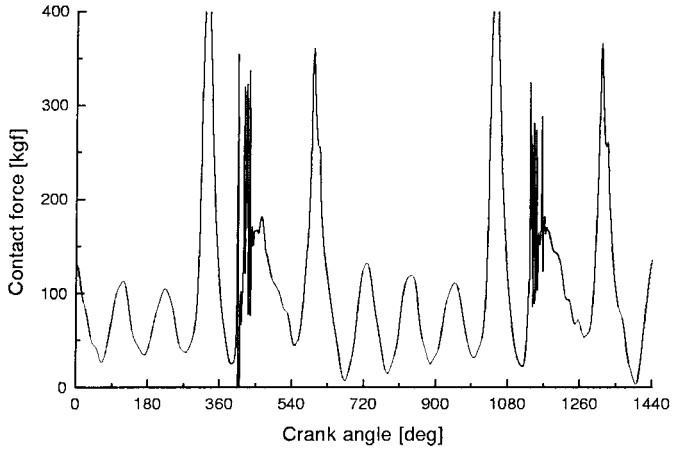

Figure 17. Contact force between roll follower and cam at the intake valve at 8300 rpm, computed with the piecewise spring model.

9. Conclusions

We present here an optimization strategy for cam design. The software obtained allows to compute cams profiles accounting for all dynamic effects present in a mechanism, including all geometrical nonlinearities of the kinematical chain.

Once the cams profile is synthetized considering different motion constraints as avoidance of interferences and limitations on maximal and minimal accelerations, the results are validated by a dynamic analysis of the full mechanism.

References

1. Bagci, C. and Kurnool, S., 'Exact response analysis and dynamic design of cam-follower systems using Laplace transforms', *Journal of Mechanical Design* **119**, 1997, 359–369.
2. Cardona, A. and Géradin, M., 'Kinematic and dynamic analysis of mechanisms with cams', *Computer Methods in Applied Mechanics and Engineering* **103**, 1993, 115–134.
3. Cardona, A., Géradin, M. and Doan, D., 'Rigid and flexible joint modelling in multibody dynamics using finite elements', *Computer Methods in Applied Mechanics and Engineering* **89**, 1991, 395–418.
4. Farouki, R., Mandunathaiah, J. and Jee, S., 'Design of rational cam profiles with Pythagorean-hodograph curves', *Mechanics Machine Theory* **33**, 1998, 669–682.
5. Grewal, P. and Newcombe, W., 'Dynamic performance of high-speed semi-rigid follower cam systems – Effects of cam profile errors', *Mechanics and Machine Theory* **23**, 1988, 121–133.
6. Hanachi, S. and Freudenstein, F., 'The development of a predictive model for the optimization of high-speed cam-follower systems with Coulomb damping internal friction and elastic and fluidic elements', *Journal of Mechanisms, Transmissions, and Automation in Design* **108**, 1986, 506–515.
7. Heizler, H., *Advanced Engine Technology*, SAE International, Warrendale, PA, 1995.
8. Heywood, J., 'Fluid motion within the cylinder of internal combustion engines – The 1986 Freeman Scholar Lecture', *Journal of Fluids Engineering* **109**, 1987, 3–35.

9. Lin, Y., Hodges, P. and Pisano, A., 'Optimal design of resonance suppression helical springs', *Journal of Mechanical Design* **115**, 1993, 380–384.
10. Lin, Y. and Pisano, A., 'General dynamic equations of helical springs with static solution and experimental verification', *Journal of Applied Mechanics* **54**, 1987, 910–917.
11. Lin, Y. and Pisano, A., 'Three-dimensional dynamic simulation of helical compression springs', *Journal of Mechanical Design* **112**, 1990, 529–537.
12. Mosier, R., 'Modern cam design', *International Journal of Vehicle Design* **23**, 2000, 38–55.
13. Neamtu, M., Pottmann, H. and Schumaker, L., 'Designing NURBS cam profiles using trigonometric splines', *Journal of Mechanical Design* **120**, 1998, 175–180.
14. Pisano, A. and Freudenstein, F., 'An experimental and analytical investigation of the dynamic response of a high-speed cam-follower system. Part 2: A combined, lumper/distributed parameter dynamic model', *ASME Journal of Mechanisms, Transmissions, and Automation in Design* **105**, 1983, 699–704.
15. Samtech, *Samcef-Mecano, User Manual*, Samtech, Liège, Belgium, 1996.
16. Schamel, A., Hammacher, J. and Utsch, D., 'Modeling and measurement techniques for valve spring dynamics in high revving internal combustion engines', in *Design of Racing and High Performance Engines*, J. Harralson (ed.), Vol. PT-53, SAE, Warrendale, PA, 1995, 83–99.
17. Srinivasan, L. and Ge, Q.J., 'Designing dynamically compensated and robust cam profiles with Bernstein–Bézier harmonic curves', *Journal of Mechanical Design* **120**, 1998, 40–45.
18. Taylor, C., *The Internal Combustion Engine in Theory and Practice*, MIT Press, Cambridge, MA, 1984.
19. Tsay, D. and Huey Jr., C.O., 'Application of rational B-splines to the synthesis of cam-follower motion programs', *Journal of Mechanical Design* **115**, 1993, 621–626.
20. Ünlüsoy, Y. and Tümer, S., 'Analytical dynamic response of elastic cam-follower systems with distributed parameter return spring', *Journal of Mechanical Design* **115**, 1993, 612–620.
21. Ünlüsoy, Y. and Tümer, S., 'Nonlinear dynamic model and its solution for a high speed cam mechanism with Coulomb friction', *Journal of Sound and Vibration* **169**, 1994, 395–407.
22. Wiederrich, J. and Roth, B., 'Dynamic synthesis of cams using finite trigonometric series', *Journal of Engineering for Industry* **97**, 1975, 287–293.
23. Yu, Q. and Lee, H., 'Influence of cam motions on the dynamic behavior of return springs', *Journal of Mechanical Design* **120**, 1998, 305–310.